

PAPER

Adaptive biohybrid pumping machine with flow loop feedback

To cite this article: Zhengwei Li et al 2022 Biofabrication 14 025009

View the article online for updates and enhancements.

You may also like

- Biohybrid Robots: Recent progress, challenges, and perspectives Victoria A. Webster-Wood, Maria Guix, Nicole W. Xu et al.
- Design, fabrication and application of magnetically actuated micro/nanorobots: a review

Zhongbao Wang, Zhenjin Xu, Bin Zhu et al.

- Thin polymeric films for building biohybrid

Leonardo Ricotti and Toshinori Fujie



Breath Biopsy® OMNI

The most advanced, complete solution for global breath biomarker analysis





Expert Study Design & Management



Robust Breath Collection



Reliable Sample Processing & Analysis



n-depth Data Analysis



Interpretation

Biofabrication



RECEIVED 16 June 2021

10 Julie 202

REVISED
5 January 2022

ACCEPTED FOR PUBLICATION
19 January 2022

PUBLISHED

4 February 2022

PAPER

Adaptive biohybrid pumping machine with flow loop feedback

Zhengwei Li¹, William C Balance², Md Saddam Hossain Joy¹, Shrey Patel³, Joanne Hwang², Hyunjoon Kong² and M Taher A Saif^{1,3},*

- 1 Department of Mechanical Science and Engineering, University of Illinois at Urbana-Champaign, Urbana, IL, United States of America
- Department of Chemical and Biomolecular Engineering, University of Illinois at Urbana-Champaign, Urbana, IL, United States of America
- Department of Bioengineering, University of Illinois at Urbana-Champaign, Urbana, IL, United States of America
- * Author to whom any correspondence should be addressed.

E-mail: saif@illinois.edu

Keywords: biohybrid machine, pump-bot, flow loop feedback, tissue engineering

Supplementary material for this article is available online

Abstract

Tissue-engineered living machines is an emerging discipline that employs complex interactions between living cells and engineered scaffolds to self-assemble biohybrid systems for diverse scientific research and technological applications. Here, we report an adaptive, autonomous biohybrid pumping machine with flow loop feedback powered by engineered living muscles. The tissue is made from skeletal muscle cells (C2C12) and collagen I/Matrigel matrix, which self-assembles into a ring that compresses a soft hydrogel tube connected at both ends to a rigid fluidic platform. The muscle ring contracts in a repetitive fashion autonomously squeezing the tube, resulting in an impedance pump. The resulting flow is circulated back to the muscle ring forming a feedback loop, which allows the pump to respond to the cues received from the flow it generates and adaptively manage its pumping performances based on the feedback. The developed biohybrid pumping system may have broad utility and impact in health, medicine and bioengineering.

1. Introduction

Almost all body functions and processes employ a variety of feedback systems [1] at molecular [2], cellular [3], organ [4], systemic [5] and whole body scales [6]. The body maintains homeostasis, such as pH [7], temperature [8], and blood flow [9] by means of the feedback control systems. A malfunction of a given regulatory feedback system will not only affect the process it governs, but also its own functions [10]. For example, the cardiovascular system is a vast network of organs and blood vessels that delivers blood to the body including the heart tissue, i.e. the heart supplies blood to itself. Thus, the pumping performance and function of the heart depends on the signals it receives from the rest of the body including any drug applied to the circulation [11].

Engineered living systems [12–14] have recently drawn significant interests, where the biohybrid machines (or 'Bio-bots') are constructed by the integration of living cells or tissues with artificial scaffolds. Due to the unique features of living components,

such as high energy efficiency, dynamic stimuli response, and self-healing or assembling properties, the developed emergent biohybrid machines or systems [15-17] have drawn significant attention. Furthermore, the engineered biomachines allow us to understand the fundamental design principles of natural organisms in a simpler and controlled *in-vitro* settings [18]. Previous studies have employed muscle cells or tissue constructs for actuation, and demonstrated bio-bots capable of walking [19–21], swimming [22–24], gripping [25–27], and pumping [28-30]. The motile bio-bots directly utilize the physiological contraction of biological components to generate the desired locomotion. On the other hand, biohybrid pumps [28–30] are developed by imparting the kinetic energy from the action of physiological contraction and transmitting that energy into the desired fluid. For example, diaphragm cardiomyocyte-driven pumps [28, 29] demonstrated feasibility of pumping liquids through microfluidic systems. Although these examples demonstrate feasibility, such pumping systems still suffer from the complicated fabrication procedures due to the involved valve or diffuser designs and poor pumping performance with extreme low flow rates in the nl min⁻¹ range. Inspired by the early embryonic heart, Li et al [30] developed a new type of skeletal muscle-powered biohybrid valveless pumpbot with impressively high flow rates reported (up to 22.5 μ l min⁻¹). An analytical model is also presented to predict the deformation and stability of circular elastic tubes subjected to a uniform squeezing force due to a muscle ring [31]. Although this pump-bot offers several merits, including ease of fabrication, simple design strategy, robustness, and high pumping performance, it is still plagued by the single pumping functionality. In fact, almost all of the biohybrid machines reported so far do not have any adaptive functionality or feedback control mechanism.

In this work, we present a skeletal musclepowered adaptive biohybrid pumping machine (pump-bot) with flow loop feedback, which can not only dynamically respond to environmental cues but also adaptively adjust its pumping performance based on the feedback. To fulfill the feedback loop control, we fabricate a polydimethylsiloxane (PDMS)/hydrogel-hybridized fluid platform consisting of a muscle ring that drives the flow, two reservoirs and tough and transparent hydrogel-based flow tubes. The pumped fluid contains acetylcholine (ACh), a biologically active molecule that affects the physiological contraction of engineered skeletal muscles. We find that the spontaneous muscle twitching can be reversibly turned OFF and ON due to addition of ACh and wash-out respectively. This Ach-triggered flow loop feedback system achieved an adaptive pumping system that could alternate between different pumping modes. The developed biological pumping system can find wide range of biomedical applications, for example, serving as an in-vitro cardiovascular pumping system for drug testing/delivery, medical diagnoses and basic physiological studies.

2. Materials and methods

2.1. Fabrication of muscle ring molds

An aluminum mold is firstly machined to serve as the template for making muscle ring molds. The detailed dimensions of the aluminum mold can be found in figures S2(A) and (B) (available online at stacks.iop.org/BF/14/025009/mmedia). PDMS is prepared by thoroughly mixing silicone elastomer (Sylgard 184) and cross-linker at 10:1 ratio by weight. The mixture is then degassed in a vacuum desiccator for at least 30 min to remove the air bubbles [30, 32]. Then PDMS prepolymer solutions are poured onto the aluminum mold and cured in the oven at 60 °C for 12 h. After carefully peeling from the Al mold, the circular PDMS structure consisting of seven circular molds with 12 mm outer diameter, 6 mm inner diameter and

3 mm depth are obtained (figure S2(A)). PDMS ring molds are cleaned by firstly sonicating in ethanol for 15 min and then autoclaving at 121 °C for 45 min in deionized water. The muscle ring molds are then blow dried and sterilized by autoclaving at 121 °C for another 45 min and 30 min drying time.

2.2. Cell culture

C2C12 mouse skeletal myoblasts (ATCC) are maintained below 60%–80% confluency in muscle growth medium (GM) consisting of Dulbecco's Modified Eagle Medium with L-glutamine and sodium pyruvate (DMEM, Corning), supplemented with 10% fetal bovine serum (Lonza) and 1% penicillinstreptomycin (Corning). To facilitate myotube formation by C2C12 myoblasts, they are cultured in muscle differentiation medium that consists of highglucose DMEM supplemented with 10% v/v horse serum (Lonza), 1% penicillin–streptomycin, and 2 mm L-glutamine (all from Gibco). C2C12 muscle cells at passage number 4 are used for making muscle rings.

2.3. Fabrication of muscle ring

For the tissue seeding procedures, extracellular matrix (ECM) solutions are prepared in the ice by first neutralizing type I collagen (Corning) with 10× phosphate buffered saline (PBS) (Lonza), 1 N sodium hydroxide (Sigma), and molecular biology grade water (Corning). Then we mix the neutralized collagen solution thoroughly with growth factor reduced Matrigel (Corning). Each collagen and Matrigel are used at the final concentration of 2 mg ml^{-1} . To fabricate muscle rings, C2C12 mouse skeletal myoblasts are suspended in ECM solution at a density of 2.5 million cells ml⁻¹. Cell-ECM mixtures are seeded into the sterilized PDMS muscle ring molds by pipetting and are polymerized at 37 °C for 30 min. Samples are then inundated in muscle GM and incubated for two days while they compact the ECM gel and form skeletal muscle rings.

2.4. Preparation of hydrogel tube

Hydrogel tubes are formed by injecting a pre-polymer solution into a glass, tube-shaped mold, allowing the solution to polymerize for 30 min, carefully removing the formed hydrogel tube, then swelling the resulting gel overnight in distilled water (figure S4(A)). The pre-polymer solution is made by briefly mixing together 1 ml of 40% w/v acrylamide, 4 μ l of 4% w/v methylene bis-acrylamide (i.e. 1:10 800 molar crosslinker ratio), $10 \mu l$ of 10% w/v ammonium persulfate, and 2 μ l of tetramethyethylene diamine. The mold is assembled by inserting a glass tube and rod into a 3D-printed polylactic acid stand with dimensions outlined in figure S4(B). The inner diameter of the glass tube was 2.1 mm, while the diameter of the glass rod is 2 mm. After swelling the resulting hydrogel tube to equilibrium in distilled water overnight, the final

dimensions of the tube are around an outer diameter of 4 mm and wall thickness of 200 μ m.

2.5. Fabrication and assembly of feedback loop pump-bots

The fluidic platform of feedback-loop pumping system is cast from machined aluminum mold (figure S1). PDMS base (Sylgard 184) and cross-linker are mixed with a 10:1 weight ratio, poured onto the aluminum mold, and degassed using a vacuum desiccator for at least 1 h. Then samples are cured in the oven at 60 °C for 12 h and carefully separated from the aluminum mold. To assemble the pumpbot, we firstly put the muscle ring onto the hydrogel tube. Then, the tube-muscle assembly is transferred into the PDMS skeleton by inserting the tube into the round PDMS channels. Pump-bot samples are inundated in muscle differentiation medium and incubated for ten days to induce the formation of myotubes inside the muscle ring.

2.6. Image acquisition

All imaging is performed on an Olympus IX81 inverted microscope (Olympus America) equipped with an environmental chamber to maintain samples at 37 °C and 5% CO₂ during the whole imaging process. The IX81 microscope is equipped with a digital CMOS camera (Hamamatsu), mounted on a vibration isolation table (Newport). For flow rate assays, green fluorescent polystyrene beads (Molecular Probes) are dispersed in cell culture media, and fluorescent images are taken at 50 fps using a $4 \times$ air objective with green fluorescent protein filter coupled to an X-Cite 120PC Q wide field fluorescent light source (Excelitas Technologies). For tube deformation analysis, the phase contrast microscope images are taken at 50 fps using a $2\times$ or $4\times$ air objective before or after adding ACh (Sigma-Aldrich).

2.7. Immunohistochemistry and confocal imaging

Before bioimaging, the muscle ring is firstly fixed with 4% paraformaldehyde in PBS for 1 h. Then, we use 0.2% Triton X-100 in PBS to permeabilize the samples for 30 min at room temperature and incubate in blocking solution consisting of 1% bovine serum albumin with 5% normal goat serum and 0.05% v/v Tween-20 in PBS for 2 h at the room temperature. Samples are then incubated overnight at 4 °C in primary antibodies (rabbit anti- α -actinin (1:250, Abcam), mouse anti-MF-20 (Developmental Studies Hybridoma Bank at the University of Iowa)) diluted in blocking solution. After washing in PBS for three times, the samples are incubated for 2 h at the room temperature in secondary antibodies (Alexa Fluor 488 goat-anti-rabbit IgG H&L (1:1000, Abcam), Alexa Fluor 647 goat-antimouse IgG H&L (1:400, Thermo Fisher Scientific)) diluted in blocking solution. To stain nuclei, samples are then incubated in 4', 6-diamidino-2-phenylindole

(DAPI) (1:1000) (Invitrogen, Carlsbad, CA, USA) for 10 min and washed with PBS again. The image acquisition is done with a confocal microscope, LSM880, using a $40\times/1.2$ NA objective lens (Carl Zeiss AG, Oberkochen, Germany). Maximum intensity projection of the acquired confocal *z*-stacks is calculated using the ImageJ software. IMARIS (Bitplane AG, Zurich, Switzerland, version 9.6.0) is used for the 3D reconstruction.

2.8. Measurement of tube deformation and flow rate

The deformation profiles of hydrogel tubes induced by cyclic muscle contractions, are measured from video recordings using the image processing software-Tracker (http://physlets.org/tracker). The trajectories of fluorescent beads inside the hydrogel tube are detected and measured by particle tracker, a 2D and 3D feature point-tracking tool for the automated detection and tracking of particle trajectories (https://imagej.net/Particle_Tracker).

3. Results

3.1. Conceptual design

The goal is to develop and test the feasibility of adaptive biohybrid pump-bot capable of managing its pumping performances based on the feedback flow. It is known that the blood is pumped by the heart to nourish the body including the heart tissue, while the pumping performance and function of the heart may depend on the content in the blood, e.g. a drug, as a feedback loop (figure 1(A)). To mimic the feedback circulatory system, we use an impedancebased pumping mechanism for the fluid transport. An impedance pump is a valveless pump which consists of a soft tube connected at both ends to a rigid tube, providing the impedance mismatch [33, 34]. By complete or partial compression of the soft tube periodically at an off-center position, a series of propagating waves is developed. These waves travel along the soft tube and get reflected back at the junctions between the soft and hard tubes with different impedances. As a result of these wave dynamics, a timeaveraged pressure gradient is established between the two ends of the gel tube, thus generating a net flow.

Inspired by this unique pumping mechanism, we propose a concept design of adaptive biohybrid pump-bot with flow loop feedback (figure 1(B)). The pump-bot is expected to have the ability to dynamically sense the environmental change and adaptively change its pumping performance based on the feedback flow. Chemicals or drugs that affect the physiological contraction of the muscle tissue can be used to mimic the environmental cues. Cyclic muscle contractions at an off-center position of the pumping system can generate unidirectional flow, and the pumped flow delivers the drugs to the muscle which affect the muscle action. The muscle action driving

Figure 1. Conceptual design of biohybrid feedback pump. (A) Schematic diagram of *in-vivo* cardiovascular system. (B) Concept design of adaptive pump-bot with flow loop feedback. (C) Biohybrid logic element achieved by the adaptive, feedback loop pump-bot.

the flow is controlled by the pumped flow, which makes it a feedback system. Potentially, such pump-bot may serve as a biological logical element which influences the output by sensing the input information (figure 1(C)).

3.2. Fabrication and biological characterization

To fulfill the feedback control, we firstly design the fluidic platform (figure 2(A)) which consists of a reservoir for the cell culture medium, inlet and outlet, and two U-shaped connecting channel to offer the flow circulation between the fluid circuit and the reservoir, and a nozzle inside the reservoir to deliver the chemicals. To construct the feedback loop platform, we first machine an aluminum mold to serve as the template for casting PDMS base. PDMS precursor and cross-linker are mixed at 10:1 ratio by weight, poured onto the aluminum mold and then cured at 60 °C for 12 h. After separating from the aluminum mold, the PDMS base fluid platform is fabricated (SI appendix, figure S1). Separately, soft and tough hydrogel tubes are fabricated by adding precursor solution of acrylamide and N, N'methylenebisacrylamide into a glass tube mold (SI appendix, figure S2). The elastic modulus of resulting hydrogel tube is roughly 10 KPa [30]. The hydrogel with a fracture energy around 2000 J m⁻² retains its structural integrity under continuous deformation [35]. The outer diameter is around 4 mm and thickness is around 200 μ m. Assembling a gel tube-muscle ring with the PDMS fluid platform forms the complete feedback loop pumping system (figure 2(B)), where the muscle ring is wrapping around the gel tube at an off-center position. Cyclic muscle contractions, spontaneous or electrically stimulated, further squeeze the tube, resulting in elastic waves that propagate along the soft gel tube and get reflected back at the soft/stiff tube boundaries. This establishes a net unidirectional fluid flow inside the soft gel tube. The flow generated by the muscle actuation returns to the muscle through the channel circuit and is delivered by the nozzle.

Muscle rings are formed by seeding living cells and ECM mixture onto circular PDMS molds with 12 mm outer diameter, 6 mm inner diameter, and 3 mm depth (SI appendix, figure S3). C2C12 mouse skeletal myoblasts are suspended at a density of 2.5×10^6 cells ml⁻¹ in a reconstituted ECM mixture of type I collagen and Matrigel® at 2 mg ml⁻¹ each and seeded into the PDMS mold (SI appendix, figure S4(A)). Upon polymerization, the collagen/Matrigel® is compacted by cellular traction forces and forms the muscle ring (figure 2(C) and SI appendix, figure S4(B)). After two days of incubation, the muscle ring is transferred onto the hydrogel tube and then incubated in muscle differentiation medium to induce formation of contractile myotubes within the muscle ring which applies a contractile force on the elastic hydrogel tube similar to a taut rubber band on a tube segment. This macroscale muscle contraction is the sum of many microscale contractions of individual myotubes acting in parallel. Therefore, aligning the axis of contractility for myotubes within muscle is thus critical to maximize the squeezing the hydrogel tube. We performed immunofluorescence staining on muscle rings to observe the alignment of the mature muscle myotubes. Anti-MF20 monoclonal antibody recognizes the light meromyosin, the rod-like tail region of myosin heavy chain protein (Developmental Studies Hybridoma Bank at the University of Iowa) and often used as a mature muscle marker. Therefore, the expression of MF-20 along with α -actinin illustrates the development of contractile apparatus assembly in muscle fiber. The alignment of myotubes in one segment of the muscle ring is along the circumferential direction imposed by the mechanical constraint of the hydrogel tube (figure 2(D)). Figure 2(E) shows the cross-striations in muscle fiber (arrow, α actinin, green), position of nuclei (DAPI, blue) and overlay of the microstructure respectively, demonstrating the integrity of functional structure of engineered skeletal muscle. 3D reconstruction of confocal z-slices of the region outlined in figure 2(D) with red cube showing the expression of (i) α -actinin, (ii) MF-20 (myosin marker), and (iii) overlay respectively (figure 2(F)). Muscle rings typically twitch spontaneously after about 10 days and last as long as 50 days in myogenic differentiation media. The muscle ring can

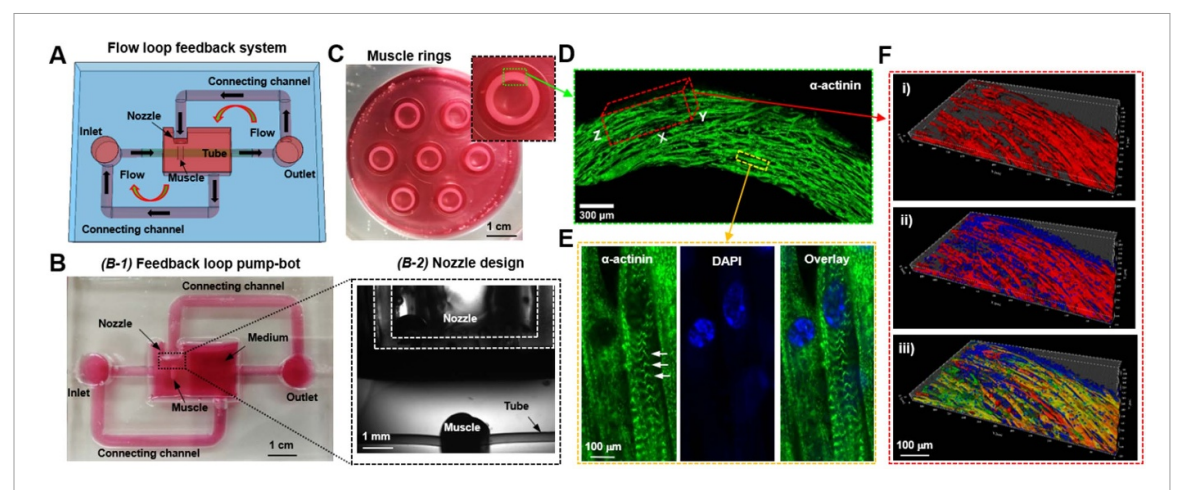


Figure 2. Design and fabrication of biohybrid feedback pump. (A) Schematic illustration of a complete adaptive pump-bot with the proposed unique flow loops. (B) Optical image of a compete adaptive pump-bot with flow loop feedback, consisting of a soft hydrogel tube connected at both ends to a feedback loop fluidic platform with a muscle ring wrapping around the hydrogel tube at an off-center position (B-1). One unique feature is the nozzle design which is used to deliver the drugs to the muscle by the feedback flow (B-2). (C) Optical image of fabricated muscle rings in the cell culture media. The *inset* highlights one muscle ring in the PDMS circular mold with a thin cap covered on the periphery (magnification: $2 \times$). (D) Maximum intensity projection of confocal z slices of a portion of muscle ring illustrating the alignment of myotube labeled with α -actinin. (E) Zoomed view of the region outlined by dotted white rectangle in (D) showing the cross-striations in a muscle fiber (arrow, α -actinin, green), position of nuclei (DAPI, blue) and overlay. (F) 3D reconstruction of confocal z-slices of the region outlined in (D) with red cube showing the expression of (i) α -actinin, (ii) MF-20 (myosin marker), and (iii) overlay.

be stimulated to contract more uniformly by applying cyclic electric field.

3.3. Pump characterization

To verify the proposed flow patterns shown in figure 2(A), fluorescent beads of 1 μ m in diameter are added to the fluid in the hydrogel tube (figure 3(B)). We use a custom designed setup that stimulates contraction of excitable cells within the muscle ring at frequencies of 4 Hz. Electric field is applied by delivering 9 V pulses with 10 ms pulse width, across two wire electrodes positioned 20 mm apart. The electrical stimulation results in a coordinated contraction of multiple myotubes within the muscle ring, which collectively generate sufficient force to deform the hydrogel tube and drive fluid flow. Unidirectional net flow is generated by the periodic muscle contraction, which is indicated by the motion of the fluorescent beads within the hydrogel tube (figure 3(B) and movie S1). Feedback flow is observed coming through the upper U-shaped channel towards the muscle (figure 3(C) and movie S2). The increased flow in the reservoir comes back to the lower U-shaped channel (movie S3). Therefore, the flow pattern displayed in figure 2(C) is experimentally verified. Furthermore, flow rate is measured by tracking the trajectories of fluorescent beads which indicate the net unidirectional flow direction. The flow pattern at electrical stimulation of 9 V and 4 Hz is parabolic, showing laminar flow. The net flow rate is obtained by $Q = \pi r^2 \bar{V} = 13.62 \ \mu l \ min^{-1}$, where \overline{V} is the average flow velocity along the tube cross section. The maximum flow velocity V_{max} is observed at the tube center and is measured to be 55.0 μ m s⁻¹. There is a streaking different types of flow forms

observed inside the hydrogel tube and in the reservoir (movie S4).

It should be noted that self-diffusion effect also induces dissemination of florescent particles from the reservoir towards the muscle ring. Thus, we quantify the relative transport due to diffusion and active pumping generated by electrical stimulation by means of the intensity change of fluorescent beads. Here, we use the ratio of the intensity of florescent beads in the muscle sitting location (region 1) to that inside the hydrogel tube (region 2), i.e. I_1/I_2 , to quantify the diffusion rate (figure 3(E)). The beads start to appear near the nozzle after around 75 min by diffusion only when there is no active pumping (no muscle) (figure 3(F) and movie S5). On the other hand, they begin to appear only after only 10 min due to the active pumping when muscle is stimulated electrically. The intensity of florescent beads in the pumping system approaches unity after around 75 min (figure 3(G)). We then quantitively measure the change of intensity ratio with the time caused by the active pumping and self-diffusion respectively. This demonstrates that the intensity change induced by the muscular pumping actuation is much faster than that caused by beads self-diffusion, indicating that the generated flow is mainly due to the muscular pumping (figure 3(H)).

3.4. Muscular response

We then use chemical/drug that affects the physiological contraction of engineered muscle tissue to mimic the native physiological cue (figure 4(A)). A PDMS platform consisting of a full reservoir and 4 mm round channels is used to test the muscular response to the drugs (figure 4(B)). Different

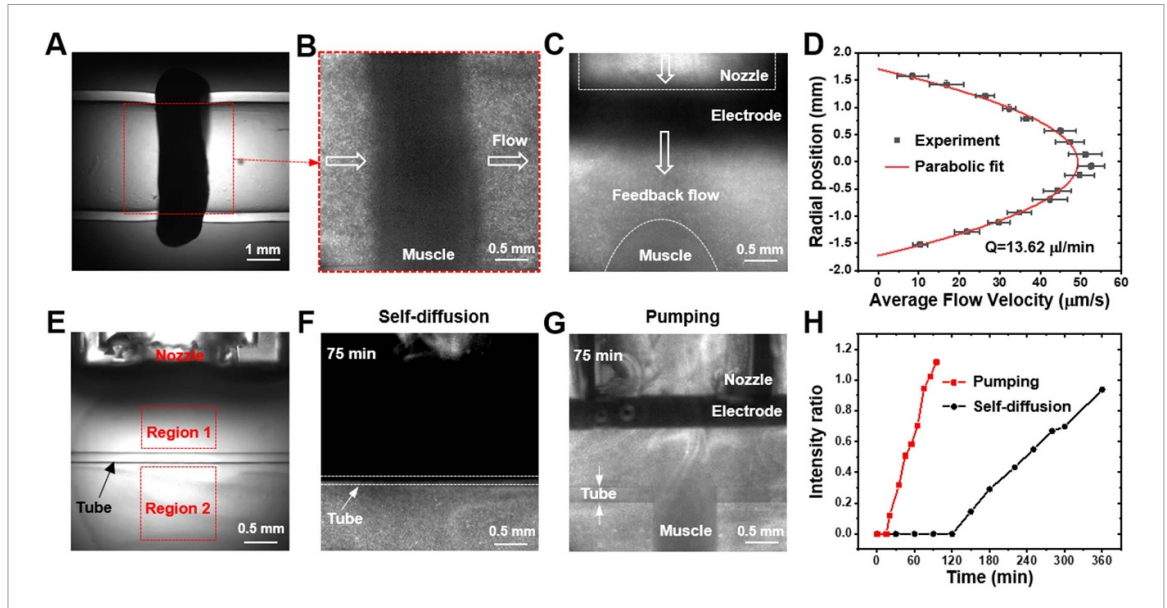


Figure 3. Characterization of feedback pumping system. (A) Phase contrast microscope image of a muscle ring wrapping around a hydrogel tube. (B) Fluorescent images of beads inside the hydrogel tube showing the unidirectional flow. (C) Fluorescent images of beads coming towards the muscle ring by means of the feedback flow. (D) Flow pattern along the diameter of hydrogel tube at the midsection, giving a net flow rate of $13.62~\mu l$ min $^{-1}$ based on the parabolic profile. (E) Phase-contrast image of the nozzle region and a half of the hydrogel tube with the florescent beads inside the tube, where the florescent image intensity ratio of region 1 versus that of region 2 used to demonstrate the feedback flow rate. (F) Fluorescent images of beads coming towards the muscle by means of the self-diffusion. (G) Fluorescent images of beads coming towards the muscle by muscular pumping under 9 V and 4 Hz electrical stimulation. (H) Intensity ratio of fluorescent beads in region 1 versus region 2 for both muscular pumping and beads self-diffusion respectively.

amounts of drug are directly added into the reservoir to test the muscular responses. The deformation of hydrogel tube near the muscle ring (as indicated by the red arrow in figure 4(C)) is used to characterize the physiological contraction of muscle ring. A representative deformation profile of the hydrogel tube induced by the spontaneous muscle twitching is shown in figure 4(D). Here, the amplitude of deformation profile A is used to characterize the strength of muscle spontaneous twitching, and the reciprocal of the contraction period 1/T to define the muscle twitching frequency. It should be noted that the strength and frequencies vary with time for the spontaneous muscle twitching.

Interestingly, we find that ACh can be used to reversibly turn off and on the spontaneous muscle twitching (figure 4(E) and movie S6). In the experiment, we firstly added 5 μ Mol ACh into the reservoir filled with 5 ml cell culture medium as shown in figure 4(B) to test the muscular response. After adding ACh, the spontaneous muscle twitching gradually decays and then completely turns off in just 15 min. After ACh washout, the muscle begins to twitch synchronously in around 5 min. Twitching becomes asynchronous after around 30 min. The muscle shows similar ON and OFF states with the second cycle of ACh application and washout. The tube deformation induced by the spontaneous muscle twitching is used to quantitatively measure the muscle twitching strength (figure 4(F), top). Muscle shows similar behavior when stimulated electrically (figure 4(F),

bottom). After adding ACh, muscle response to periodic electrical stimulation decreases rapidly, although muscle twitching does not turn off. The muscle contraction decreases quickly from the initial 46.5 μ m to 14.2 μ m in 15 min and to only 4.6 μ m in 30 min. After washout, muscle twitching can be recovered partially (figure 4(F)).

In addition to the twitching strength, the uniformity and frequency of spontaneous muscle twitching can also be tuned. Here, uniformity is defined as the ratio of standard deviation to the mean value of tube deformation. After adding ACh, the spontaneous muscle twitching becomes weaker but contractions are more uniform. After the washout, muscle first twitches uniformly and then twitching becomes non-uniform, similar to the pre-drug spontaneous twitching. Similar behavior is observed for the second cycle of ACh and washout (figure 4(G)). Regarding the twitching frequency, no significant change was observed due to the addition of Ach. After washout, the twitching frequency gradually increases and approaches the pre-ACH spontaneous twitching frequency (figure 4(H)).

To find out the threshold of muscular response to the ACh, we first add 0.5 μ Mol ACh into the 5 ml full reservoir of PDMS platform as shown in figure 4(B) and then quantitatively measure the tube deformation induced by the spontaneous muscle twitching (figure 4(I)). There was no change observed in muscle contraction after adding 0.5 μ Mol ACh even after 30 min. Next, we dispense additional 0.5 μ Mol of

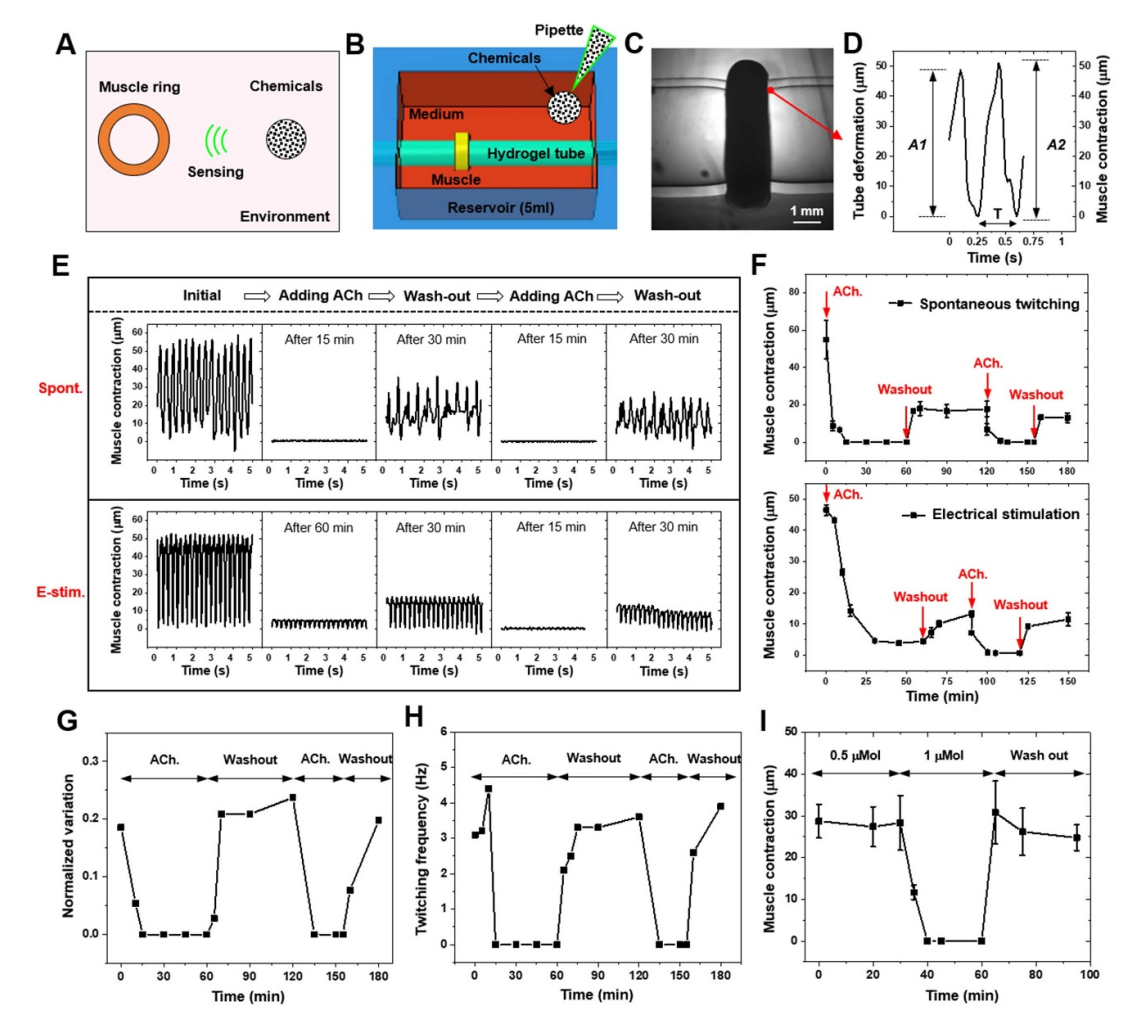


Figure 4. Muscular response to the chemical signals. (A) Schematic of muscular response to the chemicals. (B) Schematic of the setup for measuring the physiological muscle contraction. (C) Phase contrast microscope image of a muscle ring wrapping around a hydrogel tube, where the tube deformation is used to characterize the muscular response. (D) A representative tube deformation profile induced by the spontaneous muscle twitching, where the height A of the profile peaks is used to quantify the strength of muscle contraction, and the reciprocal of the contraction period 1/T to define the muscle twitching frequency. (E) The contraction profiles of both spontaneous muscle twitching and electrical stimulations at 4 Hz during the process of adding ACh and the washout. (F) The tube deformation during the whole reversible process for both spontaneous muscle twitching and electrical stimulation. (G) The uniformity of muscle twitching. (H) The muscular twitching frequency. (I) The muscular responses to different ACh concentrations.

ACh into the reservoir. In this condition, the muscle rapidly stops twitching after 10 min. After washout, the muscle twitching recovers to the initial spontaneous twitching state. Therefore, we estimate the threshold of the ACh concentration for the muscular response to be between 0.1 and 0.2 μ Mol ml⁻¹. Different tests on the muscular responses are performed, showing the repeatability and consistency (table S1).

3.5. Feedback loop and adaptive behavior

We finally add ACh into the output chamber of the flow loop feedback system to achieve adaptive behaviors (figure 5(A)). Spontaneous muscle twitching is used here to avoid any effect of artificial control mechanism on the muscle response behaviors (SI appendix, figure S5). As the muscle twitches, unidirectional net flow is observed as we expected, with a parabolic profile (figure 5(B)). The flow

rate generated by spontaneous muscle twitching is 7.76 μ l min⁻¹. And the maximum flow velocity is 29.3 μ m s⁻¹ in the middle of the cross section of the hydrogel tube. The flow fluctuates with the muscle twitching frequency, but overall movement is unidirectional. One typical trajectory and resultant flow velocity of a florescent bead at the radial position of 0.168 mm from the center of the cross section are given in figure 5(C).

There are several different stages of the adaptive behaviors observed after adding ACh into the feedback loop pumping system (figure 5(D)). Within the first 30 min, there is no obvious effect on the muscle contraction observed since the drug has not reached the muscle along the upper connecting channel in terms of the low flow velocity. Between 45 and 90 min, the muscle showed a very strong dynamic twitching behavior with very large variations (figure 5(E) and movie S7). Since the nozzle started to deliver

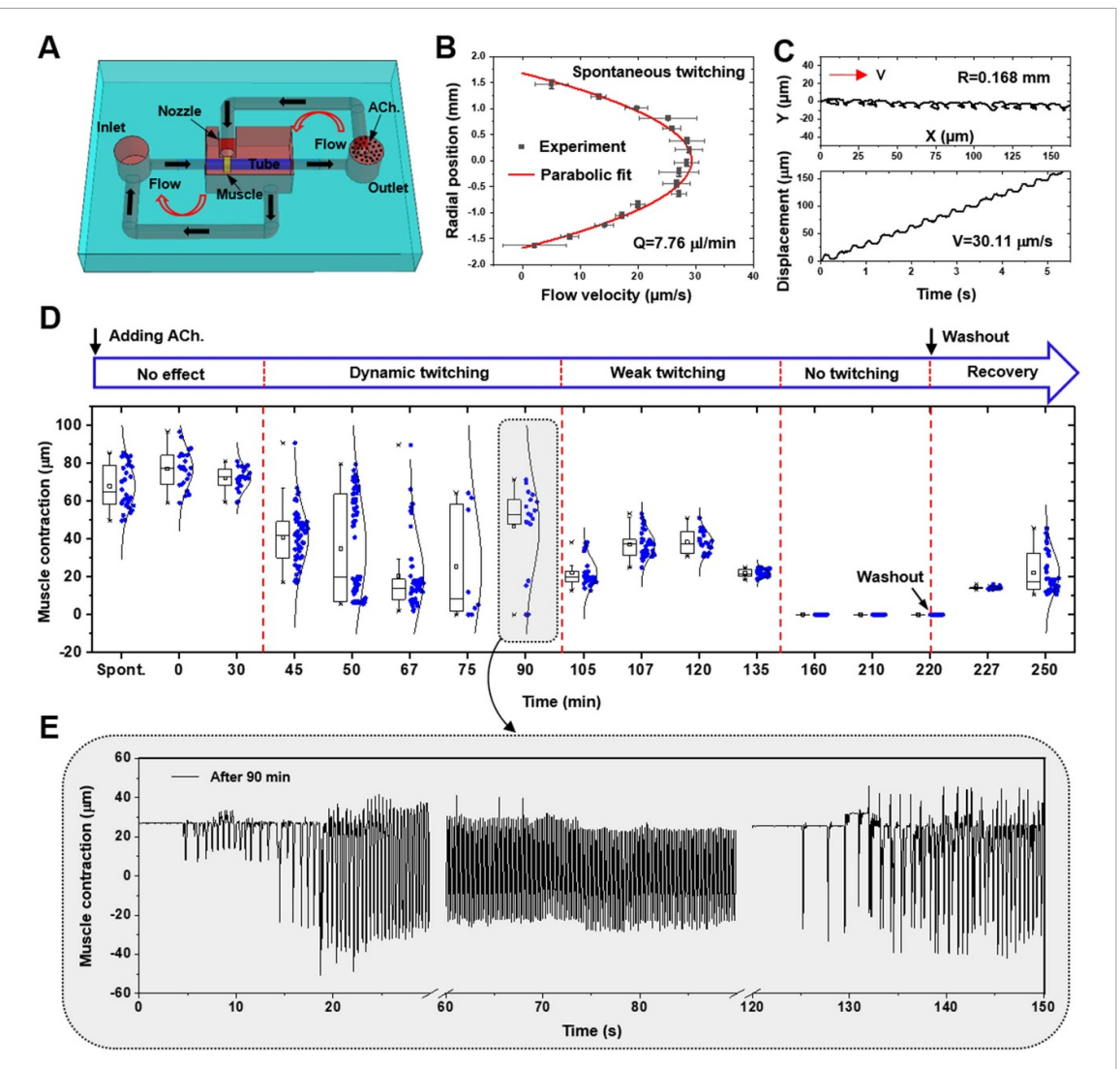


Figure 5. Feedback loop and adaptive behaviors. (A) Schematic of the feedback loop pumping system to achieve the adaptive behaviors by adding drugs into the output chamber. (B) Flow pattern generated by the spontaneous muscle twitching, following a parabolic profile. (C) Trajectory and position—time curves of florescent beads at 0.168 mm away from tube center. (D) Adaptive behaviors of muscular response after adding ACh into the feedback loop muscular pumping system. (E) Dynamic muscular response after adding ACh 90 min.

the drug to the muscle. The local drug contraction near the muscle is high while the concentration in the region farther from the muscle is low. With more drugs coming in, the drug concentration in the reservoir becomes much higher and more uniform but still below the threshold, causing the uniform but weaker muscle twitching. With further supply of drug, its concentration exceeds the threshold and shuts down the spontaneous muscle twitching. After complete washout, the spontaneous muscle twitching is restored (movie S8). Characterization with multiple samples are further performed to better understand the working and adaptive behavior by adding different amount of ACh drug into the feedback systems (figures S6 and S7). We have not achieved the self-washout functionality mainly due to the very low threshold of ACh concentration for the muscular response verified by partial washout (SI appendix, figure S8).

4. Discussion

To summarize, we report a living muscle-driven feedback loop pumping system that can dynamically sense and respond to the molecular contents of the fluid in real time by directing the flow towards the muscle. To demonstrate the concept, we designed and fabricated a unique PDMS fluid pumping platform consisting of a reservoir, two U-shaped channels that enable the flow circuit, and a soft hydrogel tube. Flow is driven by a muscle ring compressing the tube at an off-center location. Cyclic muscle contractions, spontaneous or electrically stimulated, squeeze the soft tube, resulting in elastic waves that propagate along the tube and get reflected back at the soft/stiff tube boundaries. Asymmetric placement of muscle ring results in a time delay between the wave arrivals, thus establishing a net unidirectional fluid flow inside the hydrogel tube. The flow is directed to the muscle using a nozzle.

Muscle responds to the flow depending on its contents. Consequently, pumping pattern changes. Thus, the pump becomes a feedback system. Unique circulation flow patterns are demonstrated by the pumping system, potentially mimicking the cardiovascular system. The biohybrid pumping system with flow loop feedback control may serve as a biohybrid logic element for a wide range of biomedical applications in health and medicine. For example, an in-vitro cardiovascular model can be developed by using the cardiomyocyte tissues with flow loop feedback system for physiological studies such as the effect of drugs on the 'heart' functions and performance [36, 37]. The study thus provides a foundation for developing a new class of smart biological pumping system by hybridizing living components with smart fluidic systems.

The current biohybrid pump has two limitations. First, the muscle ring is formed by a self-assembly and collagen compaction process. Hence, the rings are not identical to each other (table S2). Some of the regions of the muscle have stronger myotubes compared to the others in the same ring. As a result, muscle contraction is also non-uniform. This limitation can be overcome by improving the muscle formation protocol ensuring axisymmetry and uniform distribution of muscle cells in the cell-collagen mixture. The second limitation involves variability from one pump to the other. This is a consequence of involving living components in a device, herein the pump. Thus, even all the processes involved in making the pump are kept identical between two pumps, there resulting two pumps will have dissimilarities. This is due to the emergent property of the living component, the muscle ring. This lack of precise repeatability, as conventionally expected of engineering robots, cannot be ensured in biohybrid machines and robots.

Data availability statement

All data that support the findings of this study are included within the article (and any supplementary files).

Acknowledgments

We would like to thank Professor Roger Kamm from MIT for the helpful discussions. This project is funded by the National Science Foundation (NSF), Science and Technology Center on Emergent Behaviors in Integrated Cellular Systems (EBICS) Grant CBET-0939511, NSF CBET-1932192, and NSF Emerging Frontiers in Research and Innovation (EFRI): Continuum, Compliant, and Configurable Soft Robotics Engineering (C3 SoRo) Grant 1830881.

Author contributions

Z L, and M T A S designed research; Z L, W C B, M S H J, S P, and J H performed research; Z L, H K,

and M T A S analyzed data; Z L, and M T A S wrote the paper.

Conflict of interest

The authors declare no conflict of interest.

ORCID iDs

Zhengwei Li https://orcid.org/0000-0003-3303-0778

Hyunjoon Kong • https://orcid.org/0000-0003-4680-2968

References

- [1] Guyton A C and Hall J E 1995 Textbook of Medical Physiology 9th edn vol 9 (St. Louis, MO: W B Saunders Co)
- [2] Green G M and Lyman R L 1972 Feedback regulation of pancreatic enzyme secretion as a mechanism for trypsin inhibitor-induced hypersecretion in rats *Proc. Soc. Exp. Biol. Med.* 140 6–12
- [3] Yu Z et al 2008 A cyclin D1/microRNA 17/20 regulatory feedback loop in control of breast cancer cell proliferation J. Cell Biol. 182 509–17
- [4] Hughson R L 2003 Regulation of blood flow at the onset of exercise by feed forward and feedback mechanisms *Can*. *J. Appl. Physiol.* 28 774–87
- [5] Guyenet P G et al 2018 Interdependent feedback regulation of breathing by the carotid bodies and the retrotrapezoid nucleus J. Physiol. 596 3029–42
- [6] Mekjavic I B and Eiken O 2006 Contribution of thermal and nonthermal factors to the regulation of body temperature in humans J. Appl. Physiol. 100 2065–72
- [7] Freeman M 2000 Feedback control of intercellular signalling in development *Nature* 408 313–9
- [8] Winslow C E, Herrington L P and Gagge A P 1937 Physiological reactions of the human body to varying environmental temperatures Am. J. Physiol. 120 1–22
- [9] Holstein-Rathlou N H, Wagner A J and Marsh D J 1991 Tubuloglomerular feedback dynamics and renal blood flow autoregulation in rats Am. J. Physiol. 260 F53–F68
- [10] Singer C F, Kubista E, Garmroudi F and Cullen K J 2000 Local feedback mechanisms in human breast cancer *Breast Cancer Res. Treat.* 63 95–104
- [11] Forouhar A S *et al* 2006 The embryonic vertebrate heart tube is a dynamic suction pump *Science* 312 751–3
- [12] Kamm R D et al 2018 Perspective: the promise of multi-cellular engineered living systems APL Bioeng. 2 040901
- [13] Zhao H et al 2021 Compliant 3D frameworks instrumented with strain sensors for characterization of millimeter-scale engineered muscle tissues Proc. Natl Acad. Sci. USA 118 e2100077118
- [14] Kriegman S, Blackiston D, Levin M and Bongard J 2020 A scalable pipeline for designing reconfigurable organisms *Proc. Natl Acad. Sci. USA* 117 1853–9
- [15] Feinberg A W 2015 Biological soft robotics Ann. Biomed. Eng. 17 243–65
- [16] Ricotti L et al 2017 Biohybrid actuators for robotics: a review of devices actuated by living cells Sci. Robot 2 eaaq0495
- [17] Patino T, Mestre R and Sanchez S 2016 Miniaturized soft bio-hybrid robotics: a step forward into healthcare applications Lab Chip 16 3626–30
- [18] Raman R et al 2016 Optogenetic skeletal muscle-powered adaptive biological machines Proc. Natl Acad. Sci. USA 113 3497–502

- [19] Chan V et al 2012 Development of miniaturized walking biological machines Sci. Rep. 2 857
- [20] Cvetkovic C et al 2014 Three-dimensionally printed biological machines powered by skeletal muscle Proc. Natl Acad. Sci. USA 111 10125–30
- [21] Pagan-Diaz G J et al 2018 Simulation and fabrication of stronger, larger, and faster walking biohybrid machines Adv. Funct. Mater. 28 1801145
- [22] Williams B J, Anand S V, Rajagopalan J and Saif M T A 2014 A self-propelled biohybrid swimmer at low Reynolds number Nat. Commun. 5 1–8
- [23] Nawroth J C *et al* 2012 A tissue-engineered jellyfish with biomimetic propulsion *Nat. Biotechnol.* **30** 792–7
- [24] Park S J *et al* 2016 Phototactic guidance of a tissue-engineered soft-robotic ray *Science* **353** 158–62
- [25] Morimoto Y, Onoe H and Takeuchi S 2018 Biohybrid robot powered by an antagonistic pair of skeletal muscle tissues Sci. Robot 3 eaat4440
- [26] Akiyama Y et al 2013 Atmospheric-operable bioactuator powered by insect muscle packaged with medium Lab Chip 13 4870-80
- [27] Morimoto Y, Onoe H and Takeuchi S 2020 Biohybrid robot with skeletal muscle tissue covered with a collagen structure for moving in air APL Bioeng. 4 026101

- [28] Tanaka Y et al 2006 An actuated pump on-chip powered by cultured cardiomyocytes Lab Chip 6 362–8
- [29] Park J *et al* 2007 Micro pumping with cardiomyocyte–polymer hybrid *Lab Chip* **7** 1367–70
- [30] Li Z et al 2019 Biohybrid valveless pump-bot powered by engineered skeletal muscle Proc. Natl Acad. Sci. USA 116 1543–8
- [31] Li Z and Saif M T A 2021 Mechanics of biohybrid valveless pump-bot J. Appl. Mech. 88 111004
- [32] Li Z et al 2017 Harnessing surface wrinkling—cracking patterns for tunable optical transmittance Adv. Opt. Mater. 5 1700425
- [33] Rinderknecht D 2008 *Thesis* California Institute of Technology, Pasadena, CA
- [34] Hickerson A I, Rinderknecht D and Gharib M 2005 Experimental study of the behavior of a valveless impedance pump Exp. Fluids 38 534–40
- [35] Ballance W C et al 2020 Preoperative vascular surgery model using a single polymer tough hydrogel with controllable elastic moduli Soft Matter 16 8057–68
- [36] Yang Q et al 2021 Fabrication and biomedical applications of heart-on-a-chip Int. J. Bioprinting 7 54–70
- [37] Yang Q et al 2017 Perspective: fabrication of integrated organ-on-a-chip via bioprinting Biomicrofluidics 11 031301